ARTICLES
PUBLISHED ONLINE: 20 APRIL 2014 | DOI: 10.1038/NMAT3944
nature materials

Scalable production of large quantities of defect-free few-layer graphene by shear exfoliation in liquids

Keith R. Paton *et al.*†

To progress from the laboratory to commercial applications, it will be necessary to develop industrially scalable methods to produce large quantities of defect-free graphene. Here we show that high-shear mixing of graphite in suitable stabilizing liquids results in large-scale exfoliation to give dispersions of graphene nanosheets. X-ray photoelectron spectroscopy and Raman spectroscopy show the exfoliated flakes to be unoxidized and free of basal-plane defects. We have developed a simple model that shows exfoliation to occur once the local shear rate exceeds 10^4 s^{-1}. By fully characterizing the scaling behaviour of the graphene production rate, we show that exfoliation can be achieved in liquid volumes from hundreds of millilitres up to hundreds of litres and beyond. The graphene produced by this method performs well in applications from composites to conductive coatings. This method can be applied to exfoliate BN, MoS_2 and a range of other layered crystals.

Owing to its ultrathin, two-dimensional (2D) nature and its unprecedented properties, graphene has become the most studied of nanomaterials. In the next decade, graphene will find commercial applications in many areas from high-frequency electronics to smart coatings[1]. Some important classes of applications, such as printed electronics, conductive coatings and composite fillers, will require industrial-scale production of defect-free graphene in a processable form. For example, graphene is likely to be used as a low-cost electrode material in applications such as solar cells[2], batteries[3] and sensors[4]. Such electrodes will almost certainly be produced by solution-coating and so will require large quantities of graphene in the form of liquid suspensions, inks or dispersions[1]. Thus, liquid-exfoliation of graphene will become an important technology in the near future[5,6]. However, no scalable method exists to give large quantities of graphene that is also defect-free. For example, whereas oxidative-exfoliation of graphite can potentially give large quantities of graphene-like nanosheets, graphene oxide is typically defective[7]. Although graphene oxide has proved very useful in applications from composites to catalysis[8,9], it is very likely that an equally wide range of applications will require graphene that is free of basal-plane defects. Alternatively, sonication of graphite[10], or indeed other layered compounds[11], in certain stabilizing solvents or aqueous surfactant solutions[12,13] gives defect-free nanosheets. However, the scalability of the latter process is limited by the use of sonication as an energy source.

Thus, solution-exfoliation methods tend to exhibit either high production rates or low defect contents, but not both. A detailed literature survey (Supplementary Section 9) shows that no papers describe production rates above 0.4 g h^{-1} coupled with Raman D/G intensity ratios (a measure of defect content) below 0.65. In fact, 80% of the papers surveyed had production rates below 0.04 g h^{-1}, far too low for commercial production. One possible solution would be to find a scalable method of exfoliation that, coupled with the use of stabilizing liquids, could lead to large-scale graphene production.

Here, we demonstrate high-shear mixing (Supplementary Section 1) as a scalable alternative to sonication for the exfoliation of layered crystals such as graphite. Shear mixing is already widely used to disperse nanoparticles in liquids. However, in general this involves breaking up of nanoparticle agglomerates[14] that are weakly bound compared with the intersheet binding strength in graphite. A number of papers and patents have described methods for the exfoliation of graphite or layered compounds that incorporate shear mixing as part of the process. However, in all such cases, the layered crystal was first swelled by intercalation, significantly weakening the interlayer binding strength[15–18]. Under these circumstances, shear mixing can be used to exfoliate the crystal to give dispersed nanosheets. However, such methodologies just shift the rate-limiting step from exfoliation to intercalation, limiting the potential for scale-up. Much more useful would be the ability to exfoliate untreated layered crystals in liquids using only shear mixing. This would allow the application of the well-known strategies for the scale-up of shear-mixing processes that are commonly used in industry[19]. However, at first glance shear mixing alone seems an unlikely candidate for exfoliation of layered crystals. When using ultrasonic probes to exfoliate graphite, energy densities of thousands of watts per litre are typically used[20]. Laboratory-scale shear mixers typically deliver hundreds of watts into a few litres of liquid resulting in powder densities of ~100 W l^{-1}. Thus, one would expect exfoliation under shear to either not occur at all or to proceed at a much lower rate than sonication-induced exfoliation. However, a recent paper has shown that graphite can be exfoliated to give graphene by generating shear in a very thin liquid layer in a rapidly rotating tube[21]. However, this method gives very small quantities of graphene and is inherently un-scalable. Here we demonstrate a method for shear exfoliation of graphite to give graphene that is many times more efficient than sonication but which can be scaled-up to an industrial level. We show that shear exfoliation can produce large quantities of defect-free, unoxidized graphene and develop a model that quantitatively describes the process. In addition, this graphene performs very well in a range of applications and this method can be used to exfoliate numerous other layered crystals.

† A full list of authors and affiliations appears at the end of the paper.

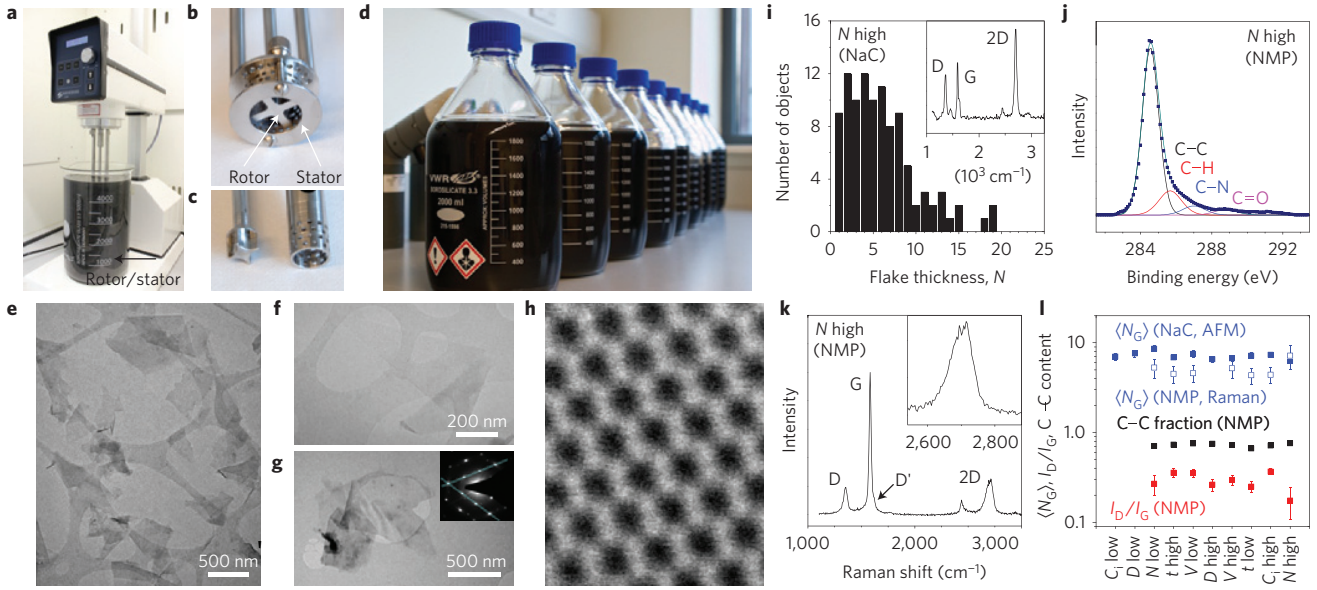

Figure 1 | Production of graphene by shear mixing. a, A Silverson model L5M high-shear mixer with mixing head in a 5 l beaker of graphene dispersion. **b**,**c**, Close-up view of a $D = 32$ mm mixing head (**b**) and a $D = 16$ mm mixing head with rotor (left) separated from stator (**c**). **d**, Graphene–NMP dispersions produced by shear exfoliation. **e**, Wide-field TEM image of SEG nanosheets (after centrifugation). **f**–**h** TEM images of individual nanosheets (**f**), a multilayer (**g**, bottom left) and monolayer (**g**, right) as evidenced by its electron diffraction pattern (**g**, inset) and a monolayer (**h**; imaged by high-resolution scanning TEM). **i**, Histogram of nanosheet thickness as measured by AFM on a surfactant-exfoliated sample. The presence of monolayers was confirmed by Raman characterization (inset). **j**,**k**, XPS (**j**) and Raman (**k**) spectra (NMP-exfoliated samples) measured on thin films. AFM, Raman and XPS analysis were performed on dispersions made using both high and low values of a given processing parameter while keeping others constant (Supplementary Section 3). The dispersion type is indicated in the panel. **l**, Information extracted from Raman, XPS and flake thickness data plotted versus dispersion type. Blue—mean flake thickness $\langle N_G \rangle$ measured by AFM for a surfactant-exfoliated dispersion and inferred from Raman for a NMP-exfoliated dispersion (Supplementary Section 3); black, fraction of XPS spectrum associated with C–C bonds; red, ratio of intensities of Raman D and G bands. The error bars represent the standard error associated with multiple measurements (~100 for AFM and ~10 for Raman). Unless noted otherwise, all data are reported for NMP dispersions.

Shear exfoliation

Shown in Fig. 1a is a Silverson model L5M mixer that generates high shear using a closely spaced (~100 μm) rotor/stator combination (Fig. 1b and Supplementary Section 1), and is available with a range of rotor diameters (Fig. 1b,c). Initial trials involved the shear-mixing of graphite both in the solvent *N*-methyl-2-pyrrolidone (NMP) and in aqueous surfactant solutions[10] (sodium cholate, NaC), resulting in large-volume suspensions (Fig. 1d and Supplementary Sections 1–3, initial processing parameters: rotor diameter, $D = 32$ mm; initial graphite concentration, $C_i = 50$ mg ml^{-1}; mixing time, $t = 20$ min; liquid volume, $V = 4.5$ l; rotor speed, $N = 4,500$ r.p.m.). After centrifugation these suspensions contain large quantities of high-quality graphene nanosheets, including some monolayers (Fig. 1e–h).

To test the effect of mixing parameters on the quality of shear exfoliated graphene (SEG), we prepared a range of dispersions using both NMP and water/NaC, keeping all but one of the mixing parameters constant (as above) but maximizing and minimizing the remaining one (Supplementary Section 3). These dispersions were studied by transmission electron microscopy (TEM) and atomic force microscopy (AFM) to measure the flake size and thickness before filtering to form ~100-nm-thick films that were characterized by X-ray photoelectron spectroscopy (XPS) and Raman spectroscopy (Fig. 1i–k and Supplementary Section 3). TEM measurements showed nanosheet sizes in the 300–800 nm range and AFM of surfactant-exfoliated samples gave typical thicknesses, N_G, of less than 10 monolayers per nanosheet ($\langle N_G \rangle \sim 5$–$8$) (Supplementary Section 3). The presence of monolayers was confirmed by Raman spectroscopy (Fig. 1i, inset). For films prepared from NMP-exfoliated graphene, XPS showed no evidence of oxidation and Raman spectroscopy reproducibly showed 2D bands (Fig. 1k, inset) consistent with N_G between 4 and 7 and a relatively weak, narrow D band (Supplementary Section 3). The Raman D/G band intensity ratio is proportional to inverse nanosheet length[22] and the D/D′ band intensity ratio[23] is ~4 (Supplementary Section 3). Taken together, these data show the D band to be dominated by nanosheet edge contributions and confirm that no basal-plane defects are introduced during exfoliation[22,23] (Supplementary Section 3). As shown in Fig. 1l, these properties were relatively invariant with mixing parameters indicating that well-exfoliated, non-oxidized, defect-free graphene can be produced using a broad range of mixing conditions. We note that these flakes are virtually indistinguishable from those produced by sonication both in terms of size and quality[10].

The exfoliation mechanism

Considering the exfoliation mechanism, our initial expectation was that localized, turbulent, highly dissipative regions were responsible for exfoliation[24,25]. However, we found turbulent energy dissipation to be unnecessary. Figure 2a maps the combinations of N and D that result in exfoliation: graphene is produced not only for turbulent, high-Reynolds-number (Re) scenarios, but also for combinations that give $\mathrm{Re}_{\mathrm{Mixer}} = ND^2\rho/\eta < 10^4$, where turbulence is not fully developed[26] (ρ and η are the liquid density and viscosity respectively). To determine whether graphene could be produced in the complete absence of turbulence, that is, under high-shear laminar flow, we shear-mixed graphite and NMP in a Couette (a concentric cylinder-based rheological cell, radius $R = 14$ mm, thickness $d = 0.1$ mm, rotation frequency of inner wall ω: shear rate $\dot{\gamma} \approx R\omega/d$, Supplementary Section 7). TEM confirmed that graphene was produced, with concentration increasing with time as $t^{0.69}$ (Fig. 2b). Interestingly, we found graphene in the Couette only

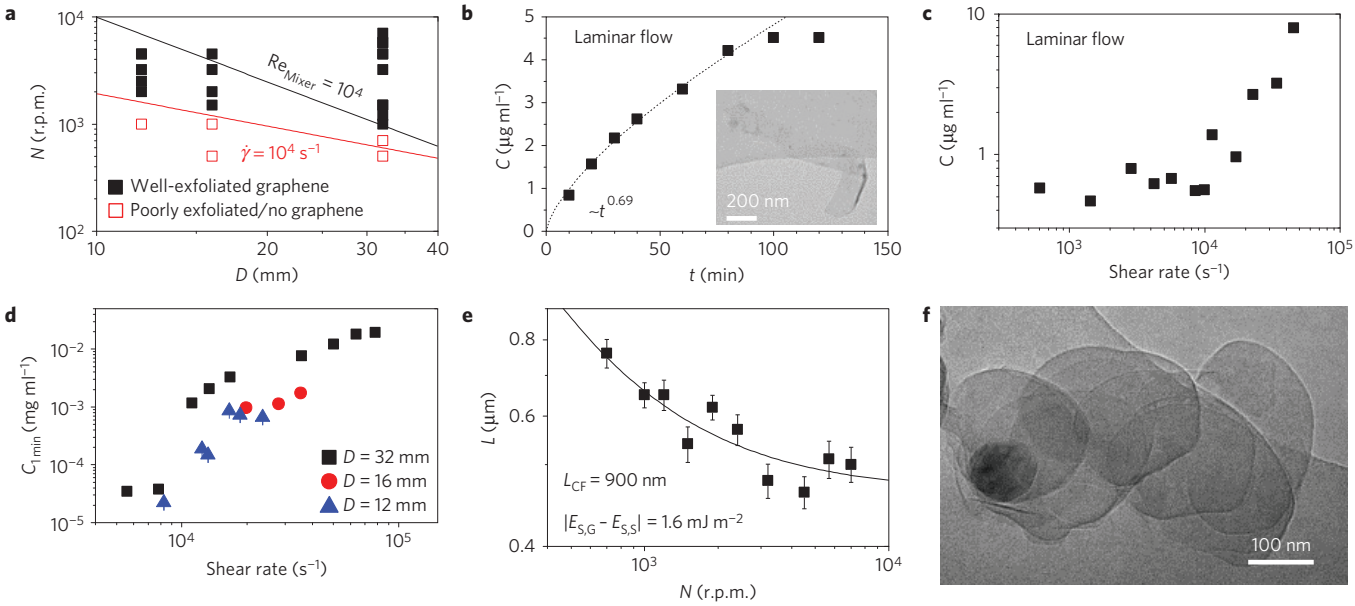

Figure 2 | Characterization of the exfoliation mechanism. a, Phase diagram of rotor speed, N, versus diameter, D, for dispersions showing good exfoliation according to TEM. The region above the black line represents fully developed turbulence, that is, $Re_{Mixer} > 10^4$, whereas the region above the red line represents $\dot{\gamma}_{min} > 10^4$ s^{-1}. **b**, Concentration (after centrifugation) of graphene produced in a rotating Couette as a function of mixing time (rotation rate 3,000 r.p.m.). Inset: TEM of Couette-produced graphene. **c**, Concentration (after centrifugation) of graphene produced in a rotating Couette as a function of shear rate (mixing time 60 min). **d**, Concentration of graphene produced in the Silverson shear mixer as a function of shear rate for rotors with diameters of 32, 16 and 12 mm (mixing time 1 min). All of three data sets are consistent with the same minimum shear rate. **e**, Mean flake length plotted versus rotor speed, N ($C_i = 50$ mg ml^{-1}; $t = 20$ min; $V = 4.5$ l; $D = 32$ mm). The error bars represent the standard error associated with ~100 measurements. The solid line is a fit to equation (2); fit constants are given in the panel. **f**, TEM image of partially exfoliated BN flake, consistent with exfoliation by shear sliding.

above a minimum shear rate of $\dot{\gamma}_{min} \approx 10^4$ s^{-1} (Fig. 2c). However, this rate is low enough to give a Re well within the laminar flow regime ($\dot{\gamma}_{min} = 10^4$ s^{-1}: $Re_{Couette} = \dot{\gamma} d^2 \rho / \eta = 60$; ref. 27) showing turbulence to be unnecessary for exfoliation.

To determine whether a minimum shear rate is a general requirement we prepared graphene in the shear mixer at a number of different N and D combinations. The concentration produced after 1 min mixing, $C_{1\,min}$, is plotted against the shear rate ($\dot{\gamma} \approx \pi ND/\Delta R$, where ΔR is the rotor–stator gap) in Fig. 2d. This suggests a minimum shear rate of $\dot{\gamma}_{min} \approx 10^4$ s^{-1}, implying that the same exfoliation mechanism occurs in both laminar and turbulent regimes. We note that all of the well-exfoliated samples in Fig. 2a are consistent with $\dot{\gamma}_{min} > 10^4$ s^{-1}. This suggests that any mixer that can achieve this shear rate can be used to produce graphene. We demonstrate this to be true by using a Kenwood kitchen blender to produce graphene. Here, exfoliation occurs because the rapidly rotating blade generates local turbulent shear rates significantly larger than 10^4 s^{-1} (Supplementary Section 4).

We can understand these processes by modelling exfoliation as shear-induced interlayer sliding in a solvent[21] (Supplementary Section 7). This predicts a minimum shear rate given by:

$$\dot{\gamma}_{min} = \frac{\left[\sqrt{E_{S,G}} - \sqrt{E_{S,L}}\right]^2}{\eta L} \quad (1)$$

where $E_{S,G}$ and $E_{S,L}$ are the surface energies of graphene and liquid ($E_{S,L} = 69$ mJ m^{-2} for NMP; ref. 10), η is the liquid viscosity (0.0017 Pa s for NMP) and L is the flake length. This equation clearly shows the role of the solvent: for solvents with surface energies matching graphene, the exfoliation energy is minimized, facilitating shear exfoliation at low shear rates. Given the flake size measured by TEM (~300–800 nm) and $\dot{\gamma}_{min} = 10^4$ s^{-1}, equation (1) predicts $E_{S,G} \approx 70.5$–71 mJ m^{-2}, very close to the expected value[10].

Equation (1) can be rewritten to express the minimum flake size that can be produced by shear exfoliation at a given $\dot{\gamma}$ (Supplementary Section 8). Then, the average flake size, $\langle L \rangle$, is approximately the mean of this value and the maximum flake size retained after centrifugation, L_{CF}. Writing the resultant equation in terms of N and D rather than $\dot{\gamma}$:

$$\langle L \rangle \approx \frac{\Delta R \left[\sqrt{E_{S,G}} - \sqrt{E_{S,L}}\right]^2}{2\eta\pi ND} + \frac{L_{CF}}{2} \quad (2)$$

Shown in Fig. 2e are data for mean flake length measured by TEM as a function of N (Supplementary Section 8). Equation (2) fits the data extremely well and gives $E_{S,G} \approx 70.6$ mJ m^{-2} and $L_{CF} = 900$ nm, close to expected values. We note that this expression also fits the data for L as a function of D (Supplementary Section 8).

This mechanism is general and does not apply only to graphite. In fact, we were able to exfoliate BN, WS_2, $MoSe_2$ and $MoTe_2$ in NMP using this mixer (Supplementary Section 5 and below). Shown in Fig. 2f is a TEM image of a partially exfoliated BN flake exhibiting laterally displaced layers consistent with the proposed shear exfoliation method[21].

Scaling up shear exfoliation

It is important to understand what controls the amount of graphene produced, with the aim of maximizing the production rate by scale-up. As properties of shear-mixed dispersions tend to scale with processing parameters as power laws[28,29], the graphene concentration should scale as

$$C \propto C_i^{\chi} t^{\tau} N^n D^d V^v \quad (3)$$

To test this, we prepared a wide range of dispersions, controllably varying all five mixing parameters. These were centrifuged and the graphene concentration measured optically (Supplementary Section 4). Keeping C_i, N, D and V constant but varying t showed $C \propto t^{\tau}$, where τ is close to 0.66 (Fig. 3a), very similar to the Couette exponent (see above and Supplementary Section 7). We note that

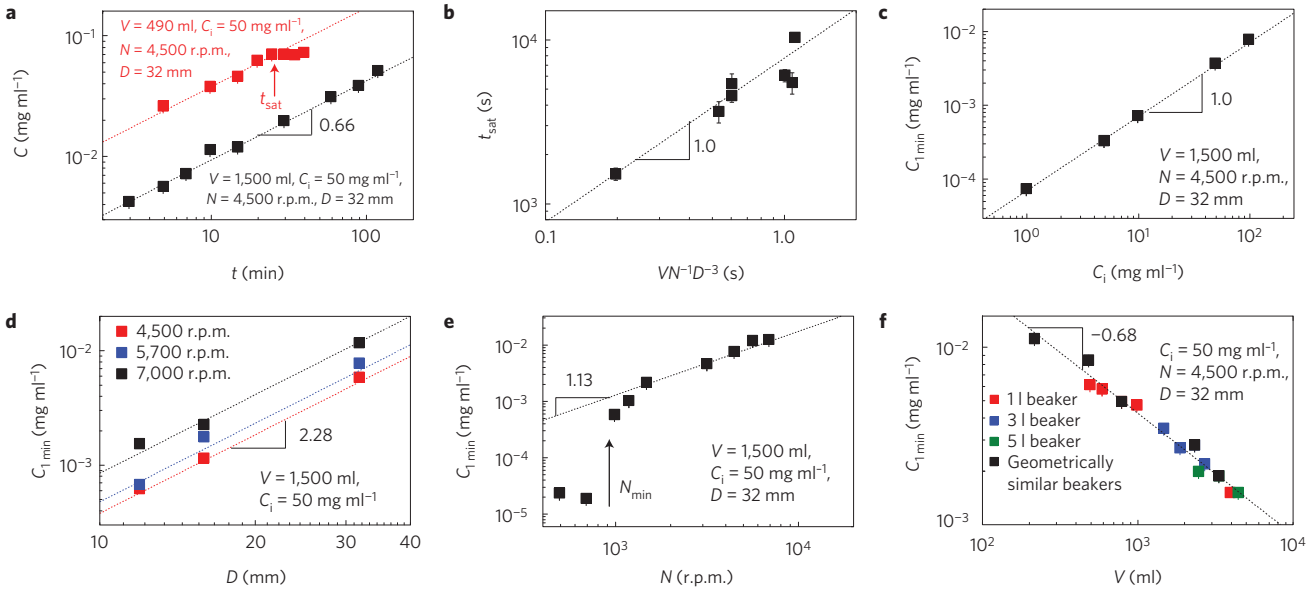

Figure 3 | Scaling of graphene production using a shear mixer. a, Dispersed concentration, C, (after centrifugation) plotted as a function of mixing time, t. The lines denote behaviour of the type: $C \propto t^{\tau}$, where τ is always close to 0.66. **b**, Graph of the measured values of saturation time, t_{sat}, plotted versus pumping time $VN^{-1}D^{-3}$. **c**–**f**, Values of graphene concentration after 1 min of mixing, $C_{1\,min}$, plotted against initial graphite concentration, C_i (**c**); rotor diameter, D (**d**); mixing speed, N (**e**) and liquid volume, V (**f**). In **c**–**f** the mixing parameters are given in the panels. In **e**, the minimum required mixing speed, N_{min}, is indicated by the arrow. In **f**, a number of beakers of different capacity, holding a range of liquid volumes, were used. Geometrically similar denotes beakers holding a specific liquid volume such that the liquid height was equal to the diameter of the beaker. The slope of the fit line is given in each panel. In all cases the errors are standard errors associated with multiple measurements as described in the Supplementary Information.

sonication-exfoliation of graphene in solvents gives $C \propto t^{1/2}$ (ref. 22), suggesting that time exponents close to 0.5–0.7 may be process-independent and so represent more fundamental behaviour.

In some cases, C saturated for times above a maximum value, t_{sat}, setting a maximum mixing time. We found t_{sat} to be proportional to $VN^{-1}D^{-3}$ (Fig. 3b), a quantity related to the time for the tank volume to be pumped through the rotor/stator once[30]. Measurements of C versus t allowed the calculation of a representative concentration for example, that achieved after 1 min mixing, $C_{1\,min}$. Measurements of $C_{1\,min}$ for different combinations of C_i, D, N and V (Fig. 3c–f) showed that power-law behaviour was observed with exponents: $\chi = 1.0$, $d = 2.28$, $\nu = -0.68$. When varying N, power-law behaviour ($n = 1.13$) was only observed above a minimum r.p.m., N_{min}, which is associated with the minimum shear rate described above.

As a result of these scaling laws, the concentration data should fall on a master curve when plotted against the scaling factor $C_i t^{0.66} N^{1.13} D^{2.28} V^{-0.68}$, as confirmed in Fig. 4a. These exponents are not specific to graphene; we plotted the concentration of MoS_2 exfoliated in NMP versus $C_i t^{0.66} N^{1.13} D^{2.28} V^{-0.68}$ (that is, using the same exponents as graphene in NMP) finding reasonable linearity (Fig. 4b).

Studies on the breakage of ceramic materials in rotor stator mixers have suggested a link between particle concentration and total energy dissipated per volume[31,32]. The power dissipated by a rotor/stator mixer is given by $P = N_P \rho N^3 D^5$ where ρ is the solvent density and $N_P \approx 2$ (ref. 26,28). This expression, coupled with the exponents measured for mixing in NMP, suggest equation (3) to be approximately equivalent to $Y = C/C_i \propto \sqrt{E/V}$, where Y is the graphene yield and E/V is the total energy dissipated per unit volume (Supplementary Section 9). Plotting Y versus E/V confirms this to be approximately true (Fig. 4c). This allows us to compare shear exfoliation to sonication-induced exfoliation (Fig. 4c), showing shear exfoliation to be considerably more efficient than ultrasonic exfoliation, becoming more so as the volume is increased (Supplementary Section 9). In addition to its inherent scalability, this result shows that shear exfoliation gives much larger quantities of graphene at lower energy cost than is possible with sonication-induced exfoliation. It is worth noting that the exfoliation yields are relatively low at <0.1%. However, by recycling graphitic sediment at least 3% of the graphite can be transformed into graphene (Supplementary Section 4). Moreover, the yield might be enhanced markedly by careful choice of the starting graphite material or optimization of the rotor.

For commercial production, the most important parameter is the graphene production rate: $P_R = VC/t$. Figure 4d demonstrates a master curve of production rate plotted versus the scaling factor $C_i t^{\tau-1} N^n D^d V^{\nu+1}$ with exponents as above. The maximum production rate achieved in laboratory trials was 1.44 g h^{-1} (for short mixing times), far higher than any rate previously achieved for solution processed defect-free graphene (Supplementary Section 9).

It will be more straightforward to scale-up shear exfoliation of graphene in aqueous rather than organic solvent environments. Thus, for large-scale studies, we focused on exfoliation by mixing in aqueous solutions of the surfactant NaC (although polymers such as polyvinylalcohol can also be used, see Supplementary Section 4). For both polymer- and surfactant-stabilized graphene, scaling behaviour was found (Supplementary Sections 4 and 6) with the data for graphene exfoliated in NaC shown in Fig. 4e. Here the scaling exponents are slightly different with $C \propto C_i t^{1.08} N^{2.54} D^{3.34} V^{-0.47}$, possibly reflecting mechanistic differences.

On scale-up, the mixing time should be fixed at $t_{sat} \propto VN^{-1}D^{-3}$, and the rotor/stator diameter should be scaled in proportion to tank size ($D \propto V^{1/3}$, see Supplementary Section 4). This predicts $P_R \propto V^{\nu+1+d/3}$, giving $P_R \propto V^{1.1}$ for NMP and $P_R \propto V^{1.6}$ for surfactant, confirming that production rate can be increased by scaling up the mixing volume. We performed large-scale trials (Fig. 4f–h), mixing in surfactant solution ($C_i = 100$ mg ml^{-1}, $t = 5$ min–4 h, $N = 3{,}000$ r.p.m., $D = 11$ cm), with volumes up to $V = 30$ l (Supplementary Section 6). This yielded up to 21 g of high-quality graphene (Raman D/G ratio of 0.18) per batch with concentrations up to $C = 0.07$ mg ml^{-1} and production rates as high as $P_R = 5.3$ g h^{-1}, significantly better than any reported work

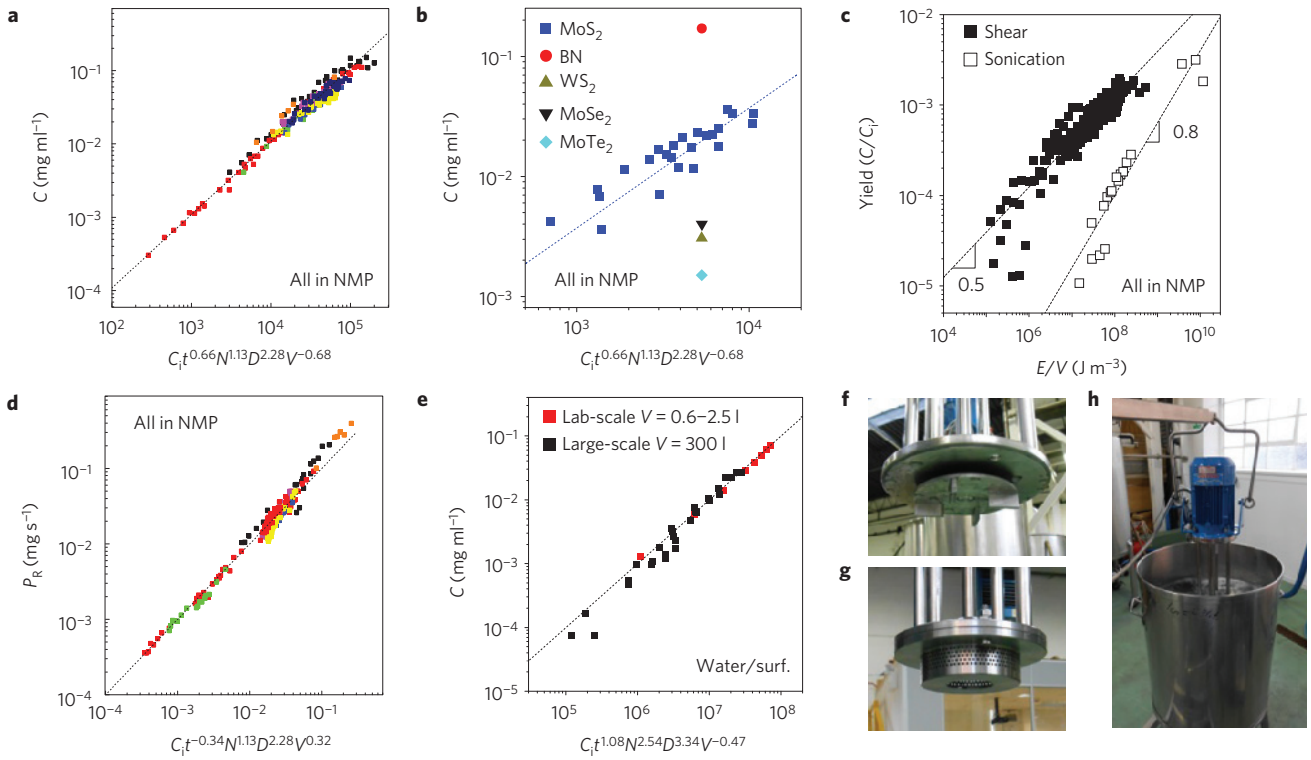

Figure 4 | Scaling of graphene production using a shear mixer. a, Graphene concentration in NMP plotted against a composite variable indicating that all data follow the scaling laws discussed in the text. **b**, Post centrifugation concentration of MoS_2 in NMP, plotted against a composite variable indicating that all data follow the scaling laws discussed in the text. Also shown in **b** are results of single trials to exfoliate BN, WS_2, $MoSe_2$ and $MoTe_2$, all in NMP. **c**, Graphene yield measured versus energy density. Also shown are equivalent data for horn-sonicated graphite (t=15–360 min, V=0.22–1 l, delivered power ~20 W). **d**, Graphene production rate in NMP plotted against the appropriate composite variable. **e**, Concentration of surfactant-exfoliated graphene plotted against a composite variable. **f**,**g**, 11-cm-diameter rotor (**f**) and stator (**g**) used during large-scale trials. **h**, Shear exfoliation of graphite in water–surfactant solution at the V=100 l scale. In **a** and **d**, the different colours represent sets of experiments performed while varying different parameters (see Fig. 3).

(Supplementary Section 6). Both laboratory-scale and large-scale concentration data followed the same scaling law (Fig. 4e). This allows us to estimate that, on scale-up to $V = 10\ m^3$, production rates exceeding $100\ g\ h^{-1}$ are possible (Supplementary Sections 4 and 6). A detailed literature review shows that no report comes close to the combination of high production rate, low Raman D/G ratio and lack of oxides reported here (Supplementary Section 9).

Applications of SEG

The SEG produced has been tested in a range of applications that require large quantities of cheap, yet good-quality graphene (Supplementary Section 10). The most obvious application is reinforcement of melt-processed composites. We added 0.07 wt% graphene to polyethylene terephthalate (PET), a common engineering plastic, by melt mixing resulting in macroscopic composites (Fig. 5a) with well-dispersed graphene nanosheets (Fig. 5b). Even at this low loading level, we found a 40% increase in strength and a 13% increase in modulus (Fig. 5c), a level of reinforcement that far surpasses that found for any other filler (Supplementary Section 10). We produced thin films of graphene nanosheets (Fig. 5d) that have conductivity as high as $400\ S\ cm^{-1}$ (Fig. 5e), competitive with other solution-processed graphenes[33] and suitable for electrode applications. One example is the replacement of the Pt/indium tin oxide electrodes in a dye-sensitized solar cell, resulting in similar levels of efficiency (Fig. 5f). Thin films (25 nm) of SEG exhibit a combination of high electrolytic capacitance at 120 Hz and phase angle close to 90° (Fig. 5g,h) suitable for use as micro-supercapacitors in electronic smoothing applications[34]. This capacitance is 10^6 times higher than nanostructured dielectric capacitors[35] and is competitive with much thicker electrodes of existing materials[36]. We have also produced novel composites by soaking commercially available elastic bands in dispersions of SEG in NMP resulting in infusion of graphene into the surface of the elastomer. This renders the band conductive with a resistance that depends exponentially on strain. Such bands make very effective dynamic strain sensors with low-strain gauge factors of ~8 and effective strain range of at least 300%, far superior to commercial metal strain gauges[37] (Fig. 5i,j).

Conclusion and outlook

We have demonstrated a scalable method for producing relatively large quantities of defect-free graphene. This was achieved using high-shear mixing, a technology that is mature, scalable and widely accessible. We have shown that exfoliation occurs whenever the local shear rate exceeds a critical value that was found to be $\sim 10^4\ s^{-1}$. Such shear rates can be achieved in a range of mixers including simple kitchen blenders. The graphene produced in this way is virtually indistinguishable from that produced by sonication of graphite in solvents or surfactants and has been demonstrated to be useful in a range of applications from composites to sensors. Importantly, high-shear mixing can also be used to exfoliate a range of other layered materials including MoS_2 and BN.

Over the past few years, it has been shown that liquid-exfoliated, 2D materials such as graphene and MoS_2 are effective in a wide range of applications from solar cells to batteries[5]. For many of these applications, commercialization will require the availability of large quantities of high-quality material. This makes the demonstration of scalable production methods for defect-free, 2D material critically

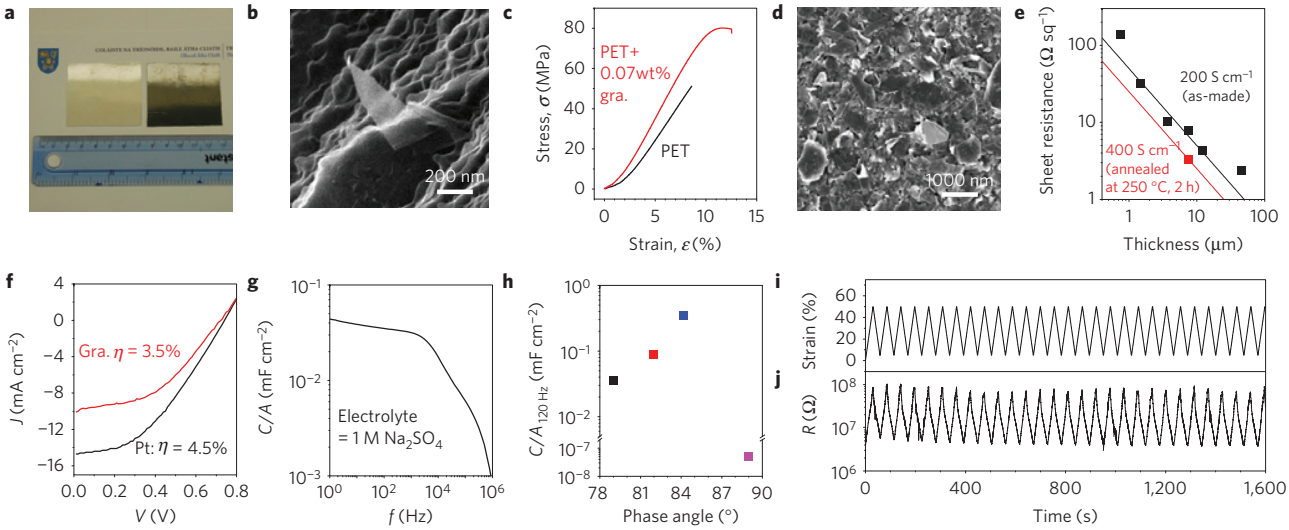

Figure 5 | Applications of mixer-exfoliated graphene. a, Melt-processed pieces of PET (left) and PET/graphene-0.07% (right). **b**, Helium ion micrograph of graphene sheet protruding from a composite fracture surface. **c**, Representative stress–strain curves of PET and PET/graphene-0.07%. **d**, Scanning electron micrograph of the surface of a vacuum-filtered graphene film. **e**, Sheet resistance versus thickness for as-made and annealed SEG films. The black and red lines illustrate the behaviour expected from films with conductivities 200 and 400 S cm^{-1} respectively. **f**, *J*–*V* curves for dye-sensitized solar cells with an indium tin oxide/Pt counter electrode (black) and a mixer-exfoliated graphene electrode (red). **g**, Areal capacitance versus frequency for a 25-nm-thick graphene electrode prepared in this work. **h**, Capacitance per unit area, measured at 120 Hz versus impedance phase angle for a 25-nm-thick graphene electrode prepared in this work (black), a 600-nm-thick graphene electrode described in ref. 36 (red), a commercial capacitive filter, on the scale of hundreds of micrometres in thickness[34] (blue), and a dielectric capacitor with nanotube electrodes (purple)[35]. **i**,**j**, Applied strain (**i**) and measured resistance (**j**) as a function of time for an elastomer/graphene composite strain sensor.

important. We believe that this work provides a significant step in that direction.

Methods

In most cases shear mixing was performed using an L5M high-shear laboratory mixer, made by Silverson Machines. The main component of the mixing head is a 4-blade rotor that sits within a fixed screen known as the stator (rotor–stator gap ~100 μm). For the Silverson LM5 mixer, rotors of diameter 12, 16 and 32 mm with rotor–stator gaps of 115, 100 and 135 μm respectively were used. The large-scale trial used much larger rotors (Supplementary Section 6). In a typical experiment, graphite powder (purchased from three different suppliers, Aldrich, FutureCarbon and Qindao Henglide Graphite, see Supplementary Section 2) was weighed into the mixing vessel, and then the exfoliating liquid was added. The mixer head was then lowered into the vessel and the speed increased gradually until the desired speed was reached. The mixer was then run at this speed for a predetermined mixing time. The main controllable mixing parameters are the rotor diameter, D (12–110 mm); the initial graphite concentration, C_i (1–100 mg ml^{-1}); the mixing time, t (3–540 min); liquid volume, V (0.2–300 l); rotor speed, N (500–7,000 r.p.m.), where the numbers in brackets represent the range of values used in this work. In this work the main exfoliating liquids were the solvent NMP and aqueous solutions of the surfactant NaC and the polymer polyvinyl alcohol. After mixing, the resultant dispersions were centrifuged (420g, 150 min) to remove any unexfoliated graphite, the supernatant collected and the graphene concentration measured optically. The mixing procedure, characterization methods and demonstration of applications potential are all described in much greater detail in the Supplementary Information.

Received 27 September 2013; accepted 11 March 2014; published online 20 April 2014

References

1. Novoselov, K. S. *et al.* A roadmap for graphene. *Nature* **490,** 192–200 (2012).
2. Kavan, L., Yum, J. H. & Gratzel, M. Optically transparent cathode for dye-sensitized solar cells based on graphene nanoplatelets. *ACS Nano* **5,** 165–172 (2011).
3. Pumera, M. Electrochemistry of graphene: New horizons for sensing and energy storage. *Chem. Rec.* **9,** 211–223 (2009).
4. Keeley, G. P. *et al.* Electrochemical ascorbic acid sensor based on DMF-exfoliated graphene. *J. Mater. Chem.* **20,** 7864–7869 (2010).
5. Nicolosi, N., Chhowalla, M., Kanatzidis, M. G., Strano, M. S. & Coleman, J. N. Liquid exfoliation of layered materials. *Science* **340,** 1226419 (2013).
6. Park, S. & Ruoff, R. S. Chemical methods for the production of graphenes. *Nature Nanotech.* **4,** 217–224 (2009).
7. Stankovich, S. *et al.* Synthesis of graphene-based nanosheets via chemical reduction of exfoliated graphite oxide. *Carbon* **45,** 1558–1565 (2007).
8. Allen, M. J., Tung, V. C. & Kaner, R. B. Honeycomb carbon: A review of graphene. *Chem. Rev.* **110,** 132–145 (2010).
9. Zhu, Y. W. *et al.* Graphene and graphene oxide: Synthesis, properties, and applications. *Adv. Mater.* **22,** 3906–3924 (2010).
10. Hernandez, Y. *et al.* High-yield production of graphene by liquid-phase exfoliation of graphite. *Nature Nanotech.* **3,** 563–568 (2008).
11. Coleman, J. N. *et al.* Two-dimensional nanosheets produced by liquid exfoliation of layered materials. *Science* **331,** 568–571 (2011).
12. Lotya, M. *et al.* Liquid phase production of graphene by exfoliation of graphite in surfactant/water solutions. *J. Am. Chem. Soc.* **131,** 3611–3620 (2009).
13. Smith, R. J. *et al.* Large-scale exfoliation of inorganic layered compounds in aqueous surfactant solutions. *Adv. Mater.* **23,** 3944–3948 (2011).
14. Wengeler, R. & Nirschl, H. Turbulent hydrodynamic stress induced dispersion and fragmentation of nanoscale agglomerates. *J. Colloid Interface Sci.* **306,** 262–273 (2007).
15. Murphy, D. W. & Hull, G. W. Monodispersed tantalum disulfide and adsorption complexes with cations. *J. Chem. Phys.* **62,** 973–978 (1975).
16. Walker, G. F. & Garrett, W. G. Chemical exfoliation of vermiculite and production of colloidal dispersions. *Science* **156,** 385–387 (1967).
17. Bunnell, L. R. Method for producing thin graphite flakes with large aspect ratios. USA patent (1993).
18. Guo, J. Low-temperature method of producing nano-scaled graphene platelets and their nanocomposites. US patent 20,080,258,359 A1 (2012).
19. Holland, F. A. & Chapman, F. S *Liquid Mixing and Processing in Stirred Tanks* (Reinhold, 1966).
20. Khan, U. *et al.* Solvent-exfoliated graphene at extremely high concentration. *Langmuir* **27,** 9077–9082 (2011).
21. Chen, X. J., Dobson, J. F. & Raston, C. L. Vortex fluidic exfoliation of graphite and boron nitride. *Chem. Commun.* **48,** 3703–3705 (2012).
22. Khan, U., O'Neill, A., Lotya, M., De, S. & Coleman, J. N. High-concentration solvent exfoliation of graphene. *Small* **6,** 864–871 (2010).
23. Eckmann, A. *et al.* Probing the nature of defects in graphene by raman spectroscopy. *Nano Lett.* **12,** 3925–3930 (2012).
24. Kresta, S. M. & Brodkey, R. S. in *Handbook of Industrial Mixing: Science and Practice* (eds Paul, E. L., Atiemo-Obeng, V. A. & Kresta, S. M.) 19–87 (John Wiley, 2004).
25. Alhassan, S. M., Qutubuddin, S. & Schiraldi, D. A. Graphene arrested in laponite-water colloidal glass. *Langmuir* **28,** 4009–4015 (2012).

26. Utomo, A. T., Baker, M. & Pacek, A. W. Flow pattern, periodicity and energy dissipation in a batch rotor-stator mixer. *Chem. Eng. Res. Des.* **86,** 1397–1409 (2008).
27. Gollub, J. P. & Swinney, H. L. Onset of turbulencein a rotating fluid. *Phys. Rev. Lett.* **35,** 927–930 (1975).
28. Hall, S., Cooke, M., Pacek, A. W., Kowalski, A. J. & Rothman, D. Scaling up of Silverson rotor-stator mixers. *Can. J. Chem. Eng.* **89,** 1040–1050 (2011).
29. Leng, D. E. & Calabrese, R. V. in *Handbook of Industrial Mixing: Science and Practice* (eds Paul, E. L., Atiemo-Obeng, V. A. & Kresta, S. M.) 639–753 (John Wiley, 2004).
30. Doran, P. M. *Bioprocess Engineering Principles* (Academic, 1995).
31. Ozcan-Taskin, N. G., Padron, G. & Voelkel, A. Effect of particle type on the mechanisms of break up of nanoscale particle clusters. *Chem. Eng. Res. Des.* **87,** 468–473 (2009).
32. Pohl, M. & Schubert, H. *Proceedings of the International Congress for Particle Technology* 1–4 (Partec, 2004).
33. De, S. & Coleman, J. N. Are there fundamental limitations on the sheet resistance and transmittance of thin graphene films? *ACS Nano* **4,** 2713–2720 (2010).
34. Lin, J. *et al.* 3-dimensional graphene carbon nanotube carpet-based microsupercapacitors with high electrochemical performance. *Nano Lett.* **13,** 72–78 (2013).
35. Sorel, S., Khan, U. & Coleman, J. N. Flexible, transparent dielectric capacitors with nanostructured electrodes. *Appl. Phys. Lett.* **101,** 103106 (2012).
36. Miller, J. R., Outlaw, R. A. & Holloway, B. C. Graphene double-layer capacitor with ac line-filtering performance. *Science* **329,** 1637–1639 (2010).
37. Li, X. *et al.* Stretchable and highly sensitive graphene-on-polymer strain sensors. *Scientific Rep.* **2,** 870 (2012).

Acknowledgements

We thank Science Foundation Ireland (11/PI/1087), the European Research Council (SEMANTICS and 2DNanoCaps), the Graphene Flagship Project (no. 604391) and Thomas Swan for financial support. We acknowledge SuperSTEM and the CRANN Advanced Microscopy Laboratory for technical support.

Author contributions

K.R.P., E.V. and P.P. performed the shear mixing and other experiments. A.O'N., M.L., P.M., R.J.S., H.P., E.L., J.C., S.E.O'B., B.M.S., E.Mc.G., T.J.P. and V.N. performed electron microscopy characterization and analysis. C.D. and A.C. performed XPS characterization and analysis. U.K., C. Boland, O.M.I., P.K., T.H. and I.A. performed applications measurements. C. Backes, N.Mc.E. and G.S.D. performed Raman and AFM analysis. S.B. and M.M. performed rheological characterization and analysis. J.N.C. designed the experiments, derived the models and wrote the paper.

Additional information

Supplementary information is available in the online version of the paper. Reprints and permissions information is available online at www.nature.com/reprints. Correspondence and requests for materials should be addressed to J.N.C.

Competing financial interests

The authors declare no competing financial interests.

Keith R. Paton[1,2], Eswaraiah Varrla[1,3], Claudia Backes[1,3], Ronan J. Smith[1,3], Umar Khan[1,3], Arlene O'Neill[1,3], Conor Boland[1,3], Mustafa Lotya[1,3], Oana M. Istrate[1,3], Paul King[1,3], Tom Higgins[1,3], Sebastian Barwich[1,3], Peter May[1,3], Pawel Puczkarski[1,3], Iftikhar Ahmed[3], Matthias Moebius[3], Henrik Pettersson[1,3], Edmund Long[1,3], João Coelho[1,4], Sean E. O'Brien[1,3], Eva K. McGuire[1,3], Beatriz Mendoza Sanchez[1,4], Georg S. Duesberg[1,4], Niall McEvoy[1,4], Timothy J. Pennycook[5,6], Clive Downing[1], Alison Crossley[6], Valeria Nicolosi[1,3,4] and Jonathan N. Coleman[1,3]*

[1]Centre for Research on Adaptive Nanostructures and Nanodevices (CRANN), Trinity College Dublin, Dublin 2, Ireland, [2]Thomas Swan and Company Limited, Rotary Way, Consett DH8 7ND, UK, [3]School of Physics, Trinity College Dublin, Dublin 2, Ireland, [4]School of Chemistry, Trinity College Dublin, Dublin 2, Ireland, [5]SuperSTEM, STFC Daresbury Laboratories, Keckwick Lane, Warrington WA4 4AD, UK, [6]Department of Materials, University of Oxford, Parks Road, Oxford OX1 3PH, UK. *e-mail: colemaj@tcd.ie